

# Evidence for higher nodal band states with $^3\text{He}$ cluster structure in $^{19}\text{Ne}$ and prerainbows in $^3\text{He}+^{16}\text{O}$ scattering

S. Ohkubo<sup>1</sup> and Y. Hirabayashi<sup>21,2</sup>

<sup>11</sup>*Department of Applied Science and Environment,  
Kochi Women's University, Kochi 780-8515, Japan*

<sup>22</sup>*Information Initiative Center, Hokkaido University, Sapporo 060-0811, Japan*

(Dated: February 16, 2022)

## Abstract

The existence of a higher nodal band state with a  $^3\text{He}$  cluster structure, i.e. a vibrational mode in which the inter-cluster relative motion is excited, in  $^{19}\text{Ne}$  in addition to those with the  $\alpha$  cluster structure in  $^{20}\text{Ne}$  and the  $^{16}\text{O}$  cluster structure in  $^{32}\text{S}$ , is suggested, which reinforces the importance of the concept of  $^3\text{He}$ -clustering in nuclei. This conclusion was reached by investigating  $^3\text{He}$  scattering from  $^{16}\text{O}$  in a wide range of incident energies and prerainbow oscillations.

The existence of an excitation mode of inter-cluster relative motion is essentially characteristic to the cluster structure in nuclei like a phonon excitation mode of the vibrational motion in spherical nuclei. The purpose of this paper is to show for the first time that this excitation, i.e. higher nodal states, exists for a  ${}^3\text{He}$  cluster by studying  ${}^3\text{He}$  scattering from  ${}^{16}\text{O}$  which shows prerainbow oscillations.

The  $\alpha$  cluster structure is widely understood in light nuclei and in the typical heavy nuclei. In contrast to an atomic molecule like the hydrogen molecule where many clear inter-atomic vibrational excitations are observed, the vibrational excitation of the inter-cluster relative motion in nuclei is rarely observed because of the weak attractive potential between the constituent clusters. The  $K = 0_4^+$  band starting at 8.6 MeV in  ${}^{20}\text{Ne}$  is an example observed in light nuclei.

On the contrary to a naive picture that the cluster structure is broken in heavier nuclei because of a strong spin-orbit potential, it is known [1, 2] that the  $\alpha$  cluster structure persists typically in  ${}^{44}\text{Ti}$  in the fp- shell region. The prediction and observation of the higher nodal bands with the  $\alpha+{}^{40}\text{Ca}$  cluster structure in  ${}^{44}\text{Ti}$  and the  $\alpha+{}^{36}\text{Ar}$  cluster structure in  ${}^{40}\text{Ca}$ , respectively [1, 2] gave further foundation to the  $\alpha$  cluster picture in heavier nuclei.

In addition to the  $\alpha$  particle,  ${}^{16}\text{O}$  is a tightly-bound doubly-magic nucleus. The famous gross structure observed in the  $90^\circ$  excitation function in  ${}^{16}\text{O}+{}^{16}\text{O}$  elastic scattering has been discussed for many years in relation to the  ${}^{16}\text{O}+{}^{16}\text{O}$  cluster structure in  ${}^{32}\text{S}$  [3], which is an analogue of  ${}^8\text{Be}$  with  $\alpha+\alpha$  structure. Different from  ${}^8\text{Be}$  and  ${}^{20}\text{Ne}$ , because of the lack of the evidence of a clear experimental rotational band with the  ${}^{16}\text{O}+{}^{16}\text{O}$  cluster structure near the threshold, whole  ${}^{16}\text{O}$  cluster aspects in  ${}^{32}\text{S}$  had not been clear. However, recently a unified description of nuclear rainbows, prerainbows and the  ${}^{16}\text{O}+{}^{16}\text{O}$  cluster structure at a low excitation energy region suggested [4] that there exists a lowest  $N = 24$  ( $N = 2n + L$  with  $n$  and  $L$  being the number of the nodes in the relative wave function and the orbital motion angular momentum, respectively) rotational band allowed by the Pauli principle and that this corresponds well to the observed band states. The famous gross resonant structures were also found to be the higher nodal states with the  ${}^{16}\text{O}+{}^{16}\text{O}$  configuration with  $N = 28$ , in which the inter-cluster relative motion is excited by two more nodes compared with the lowest  $N = 24$  band, which corresponds to the superdeformed structure in  ${}^{32}\text{S}$ .

Thus the concept of an excitation mode of the inter-cluster relative motion with a cluster structure has been established for the  $\alpha$  cluster and  ${}^{16}\text{O}$  cluster theoretically and experi-

mentally.

It is known that the  $A=3$  cluster, i.e. triton and  ${}^3\text{He}$  cluster, is also important for understanding the structure of nuclei such as  ${}^7\text{Li}$ ,  ${}^7\text{Be}$  and  ${}^{19}\text{F}$ . To reinforce the validity of the  $A=3$  cluster it is important to know if the concept of a higher nodal state is universal and if the excitation of the inter-cluster relative motion exists also for the  ${}^3\text{He}$  and  $t$  clusters. However, to the authors' best knowledge, the existence of such a higher nodal state has not been confirmed experimentally and theoretically. In fact, Waltham *et al.* [5] experimentally studied the  ${}^3\text{He}$  cluster structure in  ${}^{19}\text{Ne}$ , paying particular attention to the possible existence of higher nodal states with  ${}^3\text{He} + {}^{16}\text{O}$  structure and unfortunately reached a negative conclusion. In contrast to  ${}^{19}\text{Ne}$ , the triton cluster structure of the mirror nucleus  ${}^{19}\text{F}$  was studied theoretically by Buck and Pilt [6] with a cosh potential and by Sakuda *et al.* [7] in a semi-microscopic model and experimentally by many authors [8, 9]. However, a higher nodal state with the  $t + {}^{16}\text{O}$  configuration has not been identified.

To reveal the cluster structure of nuclei, it is very useful to study not only the low-lying bound and quasi-bound states of the composite system but also the scattering in a unified way because this checks the interaction potential not only in the surface region but also in the internal region. In fact, in this approach a long-standing controversy about the existence of the cluster structure in  ${}^{44}\text{Ti}$  was successfully solved [1, 10, 11]. As for the  $\alpha$  cluster structure in nuclei, an  $\alpha$ -nucleus potential has been studied by a systematic analysis of  $\alpha$  particle scattering from nuclei in a wide range of incident energies. For example, for the typical nuclei like  ${}^{16}\text{O}$  and  ${}^{40}\text{Ca}$ , a unique global optical potential has been established [1, 12, 13]. These systems have been a prototype for the study of the interaction potential of the composite particles and the  $\alpha$  cluster structure of the compound system. The global real potential is described well by a phenomenological potential with a form factor of Woods-Saxon squared or a folding model rather than a conventional Woods-Saxon potential [11–16]. This potential is powerful in the unified description of bound and scattering states of the composite system in the sd-shell, fp-shell and much heavier regions like  ${}^{94}\text{Mo}$  and  ${}^{212}\text{Po}$  [16, 17].

On the other hand, for  ${}^3\text{He}$  a unique global potential has not been established and a unified description of bound states and scattering has scarcely been achieved. The spin-orbit potential is an interesting and challenging subject for this system and by using a polarized beam an extensive study was done by the Birmingham group [18]. To understand

the  ${}^3\text{He}$ -nucleus interaction it is important to establish a unique global central real potential first. There are systematic experimental data of angular distributions in  ${}^3\text{He}$  scattering from  ${}^{16}\text{O}$  at  $E_L=15$  to 60 MeV [18–22]. Analyses of  ${}^3\text{He}$  scattering have been done mostly by using a conventional Woods-Saxon potential. A folding model was applied to  ${}^3\text{He}+{}^{16}\text{O}$  scattering by Khallaf *et al* [23]. However, there has been no systematic double folding model analysis of the  ${}^3\text{He}+{}^{16}\text{O}$  system from the viewpoint of a unified description of bound and scattering states.

The double folding potential we use is given as follows:

$$V_{ij}(\mathbf{R}) = \int \rho^{({}^3\text{He})}(\mathbf{r}_1) \rho^{({}^{16}\text{O})}(\mathbf{r}_2) v_{\text{NN}}(E, \rho, \mathbf{r}_1 + \mathbf{R} - \mathbf{r}_2) d\mathbf{r}_1 d\mathbf{r}_2, \quad (1)$$

where  $\rho^{({}^3\text{He})}(\mathbf{r})$  is the ground state density of  ${}^3\text{He}$  taken from Cook *et al.* [24] and  $\rho^{({}^{16}\text{O})}(\mathbf{r})$  is the nucleon density of  ${}^{16}\text{O}$ , which is obtained from the charge-density distribution determined by electron scattering [25] after the deconvolution of the proton size in the usual way, while  $v_{\text{NN}}$  denotes the DDM3Y interaction [26]. In the analysis we introduce a normalization factor  $\lambda$  for the real part of the potential and phenomenological imaginary potentials with a Woods-Saxon form factor.

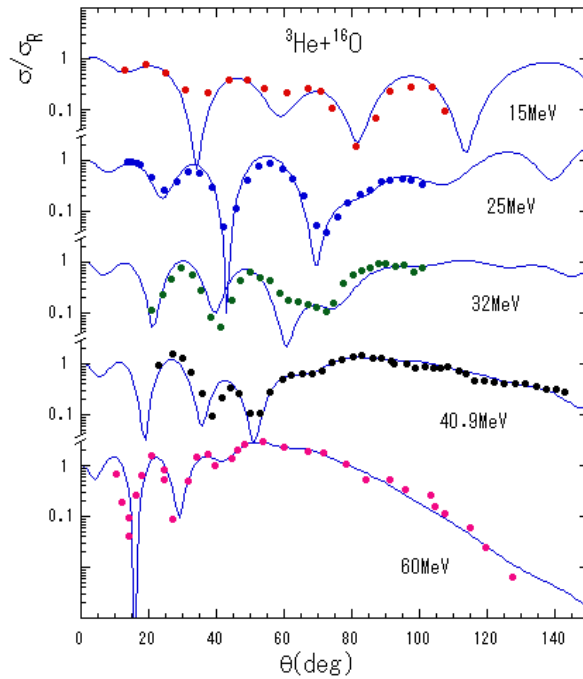


FIG. 1: (Color online) Comparison of the double folding model cross sections (solid lines) with the experimental angular distributions (points) [18–22].

In Fig. 1 calculated angular distributions of  ${}^3\text{He}+{}^{16}\text{O}$  scattering are displayed in comparison with the experimental data. In the calculations the renormalization factor  $\lambda$  and imaginary potential parameters are adjusted to fit the experimental data. The imaginary potential parameters and the properties of the real potentials used are given in Table I. The energy evolution of the characteristic angular distributions is well reproduced. At  $E_L=25$  MeV a large radius parameter of the imaginary potential is needed to fit the angular distribution beyond  $70^\circ$ . This is consistent with the analysis by Vernotte *et al.* [19]. The calculated angular distributions show some remnant of Anomalous Large Angle Scattering (ALAS) or Backward Angle Anomaly (BAA), although unfortunately there are no data at extreme backward angles. The rise at the backward angles is not so pronounced compared with typical  $\alpha+{}^{16}\text{O}$  scattering at the corresponding energies. At  $E_L=32$  MeV the angular distribution shows a prerainbow oscillation, which appears in the transitional energies from ALAS-like behavior to rainbow scattering. At  $E_L=40.9$  MeV a prerainbow oscillation is also seen with a deep minimum at  $\theta\approx 50^\circ$  and a plateau beyond. The typical fall-off of the angular distribution, which corresponds to the dark side of the rainbow, appears at  $E_L=60$  MeV with the first order Airy minimum at  $\theta\approx 27^\circ$ .

TABLE I: The normalization factor  $\lambda$ , volume integral per nucleon pair  $J_V$  of the folding potential, parameters of the imaginary potentials and its volume integral per nucleon pair  $J_W$  for the  ${}^3\text{He}+{}^{16}\text{O}$  system in the conventional notation. The calculated rms radius  $\sqrt{\langle R^2 \rangle}$  of the real potential is 3.74 fm for all the incident energies.

$E_L$ (MeV)	$\lambda$	$J_V$ (MeVfm <sup>3</sup> )	$W$ (MeV)	$R_I$ (fm)	$a_I$ (fm)	$J_W$ (MeVfm <sup>3</sup> )
15	1.24	431.6	16	4.4	0.10	119.5
25	1.23	417.7	6	5.8	0.45	108.2
32	1.24	412.9	12	4.4	0.80	118.3
40.9	1.24	408.2	12	4.5	0.90	133.1
60	1.24	388.8	12	4.6	0.80	132.4

To see the evolution of the Airy minimum the calculated angular distributions decomposed into farside and nearside contributions following the Fuller's subscription [27] are displayed in Fig. 2 (b-d) at  $E_L=32$ , 40.9 and 60 MeV. The Airy minimum is clearly seen

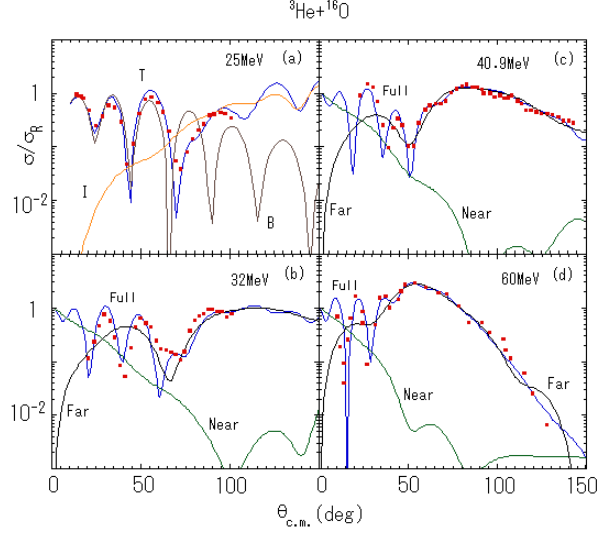


FIG. 2: (Color online) Double folding model cross sections (solid lines) are decomposed into the internal-wave (dashed lines) and the barrier-wave (dotted lines) contributions at 25 MeV (a), and the farside (dashed lines) and the nearside (dotted lines) contributions at 32, 40.9 and 60 MeV (b)-(d), and compared with the experimental data [18–22].

in each angular distribution, which shows that  ${}^3\text{He}+{}^{16}\text{O}$  scattering is transparent. This transparency can be further seen in Fig. 2(a) by decomposing the scattering amplitude into the internal-wave subamplitude, which penetrates deep into the internal region of the potential and the barrier-wave subamplitude, which is reflected at the barrier [28, 29]. Although ALAS, which is typically observed in  $\alpha+{}^{16}\text{O}$  scattering [12, 14], is not clearly seen in  ${}^3\text{He}+{}^{16}\text{O}$  scattering due to a lack of the experimental data at backward angles, there is an enhancement of cross sections at large angles in the calculated angular distributions due to the internal-wave contributions. The sharp minimum at  $70^\circ$  is due to the interference between the internal waves and the barrier waves and is a prototype of the Airy minimum of the prerainbow at 32 MeV and the rainbow at 60 MeV in Fig. 2(b)-(d).

The obtained real potential should work at the bound and quasi-bound energy region as was demonstrated in the typical  $\alpha+{}^{16}\text{O}$  and  $\alpha+{}^{40}\text{Ca}$  systems [1]. The potential determined at  $E_L=15$  MeV locates the lowest Pauli-allowed ground state of  ${}^{19}\text{Ne}$  with the  ${}^3\text{He}+{}^{16}\text{O}$  configuration at  $-4.97$  MeV from the  ${}^3\text{He}$  threshold, which falls well within the range of the experimental energy  $-8.44$  MeV. As seen in Table I, the volume integral of the folding potential shows a tendency to increase as the energy decreases, which arises from the energy

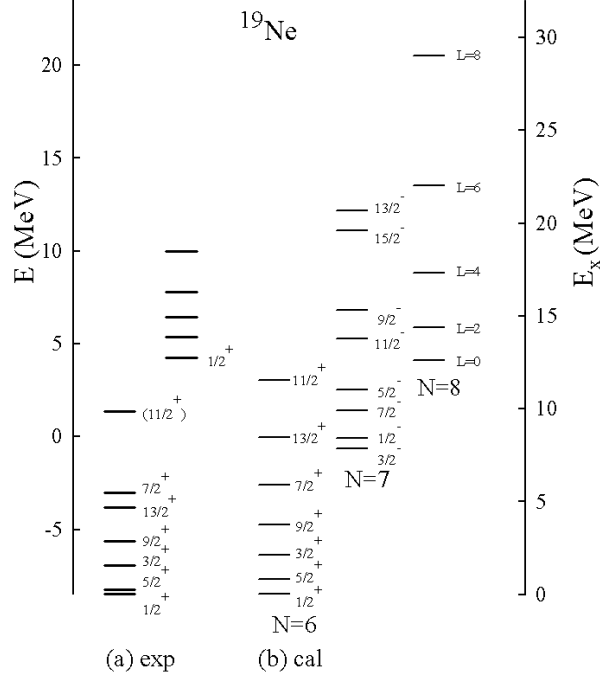


FIG. 3: (a) The experimental  $^3\text{He}$  cluster state candidates in  $^{19}\text{Ne}$  [5, 8, 9, 30] ; (b) The  $N = 6$ ,  $N = 7$  and  $N = 8$  states supported by the double folding potential (the potential is fixed to the folding potential at  $E_L=15$  MeV with  $\lambda=1.34$ ). Energies are given with respect to the  $^3\text{He}+^{16}\text{O}$  threshold (left) and in excitation energy (right). For the  $N = 8$  band the energies where the phase shift passes  $270^\circ$  for  $L = 4, 6$  and  $8$ , and the energies where the phase shift approaches the highest for  $L = 0$  and  $2$ , are displayed.

dependence of the DDM3Y interaction. To reproduce the experimental ground state energy  $\lambda=1.34$  is used ( $J_V=466.4$  MeVfm $^3$ ) and the calculated energy levels are displayed in Fig. 3. The double folding potential used is shown in Fig. 4. In the calculation the following spin-orbit potential is introduced:

$$V_{so}(R) = -V_{so} \left( \frac{\hbar}{m_{\pi}c} \right)^2 \frac{1}{R} \frac{dV(R)}{dR} \vec{L} \cdot \vec{\sigma}, \quad (2)$$

where  $\vec{\sigma}$  is the spin of the  $^3\text{He}$  cluster. The strength constant  $V_{so} = 0.011$  MeV is used to fit the splitting of the  $\frac{5}{2}^+$  ( $E_x=0.238$  MeV) and  $\frac{3}{2}^+$  (1.576 MeV) states. The calculated ground band with  $N = 6$  corresponds well to the experimental levels. The ground band has a rather shell-like structure and  $^3\text{He}$  clustering is not strong. The ( $\frac{11}{2}^+$ ) state at  $E_x=9.8$  MeV was observed in  $^3\text{He}$ -transfer reactions [30]. The  $^3\text{He}$  cluster strength of the experimental high spin states  $\frac{11}{2}^+$  and  $\frac{13}{2}^+$  of the ground band could be shared over two or more states as

in  $^{19}\text{F}$  [6] and the theoretical  $\frac{11}{2}^+$  and  $\frac{13}{2}^+$  states in Fig. 3 could be the centroid of them. As a parity doublet partner of the ground band, the  $N = 7$  negative parity band with the  $^3\text{He}+^{16}\text{O}$  cluster structure whose band head  $\frac{3}{2}^-$  state starts just near the  $^3\text{He}$  threshold is predicted. In the mirror nucleus  $^{19}\text{F}$ , some of the member states of the  $N=7$  band with the  $t+^{16}\text{O}$  cluster structure have been identified in the cluster model calculations by Buck and Pilt [6] and Sakuda *et al.* [7]. The  $(\frac{7}{2}^-)$  state in  $^{19}\text{Ne}$  at 6.861 MeV, which is an isospin-analog state of the  $N = 7, \frac{7}{2}^-$  state at 6.927 MeV in  $^{19}\text{F}$  [6, 7, 31] could be a member state of the  $N = 7$  band in  $^{19}\text{Ne}$ . Sakuda *et al.* [7] pointed out that to reproduce the experimental energy levels of the  $N=7$  negative parity band correctly the coupling between the cluster states with the  $t+^{16}\text{O}$  configuration and the cluster states with the  $\alpha+^{15}\text{N}^*$  configuration is important, which will also hold in  $^{19}\text{Ne}$ . Very recently Yamazaki *et al.* [32] claim that they observed three low-lying members of the negative parity rotational band in the  $^{16}\text{O}(^6\text{Li},t)$  transfer reactions. Although no details are given in Ref.[32], it could be that these correspond to member states of the  $N = 7$  parity doublet band.

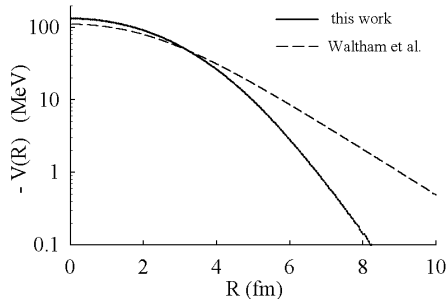


FIG. 4: Comparison of our central double folding potential used in Fig. 3 (solid line) with the cosh potential of Waltham *et al* [5] (dashed line).

In order to investigate the cluster states above the threshold phase shifts calculated with this potential (by switching off the spin-orbit potential) are displayed in Fig. 5. It is noticed that the phase shifts for even parity and odd parity show very different behavior. The phase shifts for even parity increase toward  $270^\circ$  and the  $L=4, 6$  and  $8$  show broad resonant behavior. On the other hand, for odd parity there appears no resonant behavior to approach  $270^\circ$ . This different behavior of the even and odd parity phase shifts is very similar to the case for the  $\alpha+^{16}\text{O}$  system.

In  $^{20}\text{Ne}$  the corresponding states with  $N = 10$  with a developed  $\alpha+^{16}\text{O}$  cluster structure

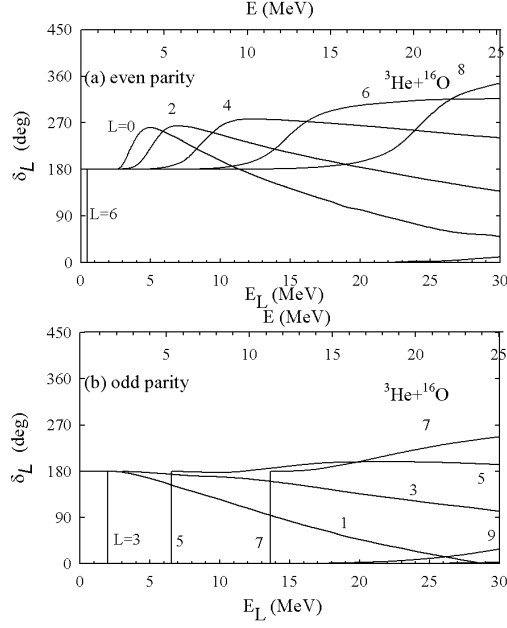


FIG. 5: Phase shifts calculated with the double folding potential used in the energy level calculations in Fig. 3.

have one more node compared with the  $N = 8$  ground band wave functions. It was pointed out [14] that although the high spin  $6^+$  and  $8^+$  states of the higher nodal  $N = 10$  band are difficult to be observed as an individual energy level because of its large width, its persistent existence can be seen in the phenomenon of BAA or ALAS in  $\alpha+^{16}\text{O}$  scattering. The  $N = 8$  band with the  $^3\text{He}+^{16}\text{O}$  cluster structure in  $^{19}\text{Ne}$  is an analogue of the higher nodal band in  $^{20}\text{Ne}$ . As seen in Fig. 2(a), the sharp Airy minimum of the prerainbow oscillation at  $70^\circ$  in the angular distribution at  $E_L=25$  MeV, which clearly separates the two components of the amplitude responsible for the Airy structure, is caused by the interference between the internal waves, which are mostly due to the existence of the high spin members of the higher nodal band and the barrier waves.

Based on the above picture, the experimental results of Waltham *et al.* [5] in  $^{16}\text{O}(^3\text{He},\gamma)$  capture reactions and the old  $^3\text{He}$  elastic scattering data at  $E_L=5.05$  MeV by Röpke *et al.* [33] can now be understood quite naturally as the experimental evidence for the existence of the  $N = 8$  higher nodal states. Firstly the  $\frac{1}{2}^+$  state at  $E_x=12.69$  MeV observed in the measurement of  $^3\text{He}+^{16}\text{O}$  elastic scattering at  $E_L=5.05$  MeV ( $E=4.25$  MeV) [9, 33] well corresponds to the calculated higher nodal state with  $L = 0$  (Fig. 3). This state has a large  $^3\text{He}$  decay width  $\Gamma_{c.m.}/\Gamma_{tot}=0.43$  with  $\Gamma_{c.m.}=0.18$  MeV [33] in accordance with the character

of the higher nodal member state. Secondly as for the experimental results of Waltham *et al.* [5], they performed an experiment to search for highly excited  ${}^3\text{He}$  cluster states in  ${}^{19}\text{Ne}$  and discussed the newly observed energy levels in comparison with the cluster model calculations with a cosh potential of Buck and Pilt [6]. They reached the conclusion that the cluster model is unsuccessful in the highly excited energy region [5]. However, we note that the cosh potential they used has an unphysical long tail as seen in Fig. 4 (the volume integral is  $695 \text{ MeVfm}^3$ !) and is not appropriate for the description of the energy levels of the highly excited cluster states and  ${}^3\text{He}+{}^{16}\text{O}$  scattering. In fact, their calculated energy levels are located at energies which are lower than they should be if an appropriate potential is used. (The drawback of this long tail of the cosh potential has already been discussed for the  $\alpha+{}^{40}\text{Ca}$  system [34].) Although they tried to interpret their observed states as member states of the  $N = 9$  band unsuccessfully, the observed energy levels should be regarded as the  $N = 8$  higher nodal states with  $L = 2, 4$  and  $6$ . The correspondence between the observed states and the present calculation is good as seen in Fig. 3. The observed states at  $E_x=13.8, 14.88$  and  $16.24 \text{ MeV}$  have comparable widths  $\Gamma_{c.m.}=0.67, 0.62$  and  $0.40 \text{ MeV}$ , respectively and have a large  $L = 2$  contribution in the Legendre polynomial analysis of the angular distributions of the  ${}^{16}\text{O}({}^3\text{He},\gamma)$  capture cross sections [5]. These states may be considered to be fragmented from the higher nodal  $L = 2$  state. (The centroid energy is  $15 \text{ MeV}$ .) The state at  $E_x=18.4 \text{ MeV}$  with  $\Gamma_{c.m.}=4.4 \text{ MeV}$  [5] has a broad resonant structure and may be considered as a candidate for the member state of the higher nodal band with  $L = 4$ . The dimensionless reduced width  $\theta^2$  (defined by  $\Gamma = 2P_L(a)\gamma_W^2(a)\theta^2(a)$ , with  $P$  the Coulomb penetrability,  $\gamma_W^2$  the Wigner limit value and  $a$  the channel radius) calculated at a channel radius  $5 \text{ fm}$  is  $\theta^2 = 0.20, 0.13$  and  $0.07$  for the  $E_x=13.8, 14.88$  and  $16.24 \text{ MeV}$  states respectively, assuming  $L = 2$  and  $\theta^2=1.0$  for the  $E_x=18.4 \text{ MeV}$  state assuming  $L = 4$ , which is compatible with the present picture. The rotational constant of the calculated  $N = 8$  band,  $k \simeq 0.21$ , is comparable with  $k \simeq 0.24$  estimated from the experimental centroid at  $E_x=15 \text{ MeV}$  ( $L = 2$ ) and the  $18.4 \text{ MeV}$  ( $L = 4$ ) state. Yamazaki *et al.* [32] claim that they observed six prominent peaks above  $E_x= 12 \text{ MeV}$  in the  ${}^{16}\text{O}({}^6\text{Li},t)$  transfer reactions. It is interesting to know whether these could be fragmented states of the  $N = 8$  higher nodal band.

To summarize, the existence of the  $N = 8$  higher nodal band states with the  ${}^3\text{He}+{}^{16}\text{O}$  cluster structure in  ${}^{19}\text{Ne}$ , in which inter-cluster relative motion is excited, was strongly sug-

gested by studying  ${}^3\text{He}+{}^{16}\text{O}$  scattering which shows prerainbow oscillations. The calculated low spin members of the higher nodal band states with  $L = 0$  correspond well with the observed state in the low energy  ${}^3\text{He}$  elastic scattering at  $E_L=5.05$  MeV [9, 33] and the states with  $L = 2, 4$  and  $6$  correspond well to the observed states in the  ${}^{16}\text{O}({}^3\text{He},\gamma)$  capture reactions [5]. A higher nodal band state may appear more clearly and stably in  ${}^{19}\text{Ne}$  than in  ${}^{20}\text{Ne}$  due to coupling to the other states nearby. In the mirror nucleus  ${}^{19}\text{F}$  a similar higher nodal band with the  $t+{}^{16}\text{O}$  cluster structure and prerainbow oscillations in  $t+{}^{16}\text{O}$  scattering are expected. The present findings about the higher nodal band states with the  ${}^3\text{He}$  cluster in  ${}^{19}\text{Ne}$  in addition to the higher nodal states with the  $\alpha$  cluster structure in the  ${}^{20}\text{Ne}$ ,  ${}^{40}\text{Ca}$  and  ${}^{44}\text{Ti}$  nuclei and the higher nodal states with the  ${}^{16}\text{O}$  cluster structure in the  ${}^{32}\text{S}$  nucleus reinforce the importance of the concept of the higher nodal state and the  ${}^3\text{He}$  cluster in nuclei.

One of the authors (S.O.) has been supported by a Grant-in-aid for Scientific Research of the Japan Society for Promotion of Science (No. 16540265) and the Yukawa Institute for Theoretical Physics .

- 
- [1] F. Michel, S. Ohkubo, and G. Reidemeister, *Prog. Theor. Phys. Suppl.* **132**, 7 (1998); and references therein.
  - [2] T. Yamaya, K. Katori, M. Fujiwara, S. Kato, and S. Ohkubo, *Prog. Theor. Phys. Suppl.* **132**, 73 (1998); and references therein.
  - [3] A. Gobbi and D. A. Bromley, in: R. Bock (Ed.) *Heavy Ion Collisions*, Vol. 1, North-Holland, Amsterdam, 1979, p.485 and references therein.
  - [4] S. Ohkubo and K. Yamashita, *Phys. Rev. C* **66** (2002) 021301(R).
  - [5] C. E. Waltham, S. H. Chew, J. Lowe, J. M. Nelson, and A. R. Barnett, *Nucl. Phys.* **A395**, 119 (1983).
  - [6] B. Buck and A. A. Pilt, *Nucl. Phys.* **A280**, 133 (1977).
  - [7] T. Sakuda and F. Nemoto, *Prog. Theor. Phys.* **62**, 1274 (1979); **62**, 1606 (1979); H. Furutani *et al.*, *Suppl. Prog. Theor. Phys.* **68**, 193 (1980); and references therein.
  - [8] M. Hamm, C. W. Towsley, R. Hanus, K. G. Nair, and K. Nagatani, *Phys. Rev. Lett.* **36**, 846 (1976).

- [9] D. Ajzenberg-Selove, Nucl. Phys. **A475**, 1 (1987); **A392**, 1 (1983); **A300**, 1 (1978); ENSDF database (Evaluated Nuclear Structure Data File), <http://www.nndc.bnl.gov/ensdf/>.
- [10] F. Michel, G. Reidemeister, and S. Ohkubo, Phys. Rev. Lett. **57**, 1215 (1986).
- [11] S. Ohkubo, Phys. Rev. C **38**, 2377 (1988).
- [12] F. Michel *et al.*, Phys. Rev. C **28**, 1904 (1983).
- [13] Th. Delbar *et al.*, Phys. Rev. C **18**, 1237 (1978).
- [14] S. Ohkubo, Y. Kondo, and S. Nagata, Prog. Theor. Phys. **57**, 82 (1977).
- [15] H. Abele and G. Staudt, Phys. Rev. C **47**, 742 (1993).
- [16] U. Atzrott *et al.*, Phys. Rev. C **53**, 1336 (1996).
- [17] S. Ohkubo, Phys. Rev. Lett. **74**, 2176 (1995).
- [18] Y. -W. Lui *et al.*, Nucl. Phys. **A333**, 205 (1980).
- [19] J. Vernotte *et al.*, Nucl. Phys. **A390**, 285 (1982).
- [20] L. Alvarez and G. Pállá, J. Phys. **G 8**, 987 (1982).
- [21] V. V. Adodin, N. T. Burtebaev, and D. Duisebaev, Sov. J. Nucl. Phys. **55**, 319 (1992).
- [22] H.-J. Trost, P. Lezoch, and U. Strohbush, Nucl. Phys. **A462**, 333 (1987); see also references therein.
- [23] S. A. E. Khallaf, A. M. Amry, and S. R. Mokhtar, Phys. Rev. C **56**, 2093 (1997).
- [24] J. Cook and R. J. Griffiths, Nucl. Phys. **A366**, 27 (1981).
- [25] H. de Vries *et al.*, At. Data Nucl. Data Tables **36**, 495 (1987).
- [26] A. M. Kobos *et al.*, Nucl. Phys. **A425**, 205 (1984).
- [27] R. C. Fuller, Phys. Rev. C **12**, 1561 (1975).
- [28] D. M. Brink, *Semi-classical Methods for Nucleus-Nucleus Scattering* (Cambridge University Press, Cambridge, 1985).
- [29] J. Albiński and F. Michel, Phys. Rev. C **25**, 213 (1982).
- [30] L. Kraus *et al.*, Phys. Rev. C **37**, 2529 (1988).
- [31] Utku *et al.*, Phys. Rev. C **57**, 2731 (1998).
- [32] A. Yamazaki *et al.*, Abstract Book of *The Cluster Conference*, 3-7 Sept., 2007, Stratford Upon Avon, UK (2007) p.95.
- [33] H. Röpke, K.P. Lieb, and R. König, Nucl. Phys. **A97**, 609 (1967).
- [34] S. Ohkubo, Phys. Rev. C **39**, 1186 (1989).